An enriched finite element for crack opening and rebar slip in reinforced concrete members

Loredana Contrafatto, Massimo Cuomo, Francesco Fazio

An enriched finite element for crack opening and rebar slip in reinforced concrete members

Loredana Contrafatto · Massimo Cuomo · Francesco Fazio

Abstract Object of the paper is the simulation of reinforced concrete bars behaviour, accounting for crack opening and concrete-rebar slippage. A macro beam element with a single uniform reinforcement is studied in details in the uniaxial case. Distinct constitutive hypotheses are formulated for the materials. The CEB-FIP Model Code 90 rules the behaviour of the materials interface that is assumed to be fully dissipative. Steel is supposed to behave elastoplastically with hardening. Crack opening in the concrete matrix is introduced by means of a strong discontinuity approach (SDA). All the relevant equations of the problem are variationally derived from a mixed energy functional. Two enhancements of the enriched kinematics, based on polynomial or exponential shape functions, respectively, are compared with the usual SDA enhancement. As an alternative approach, high-order interpolation of the displacement field based on B-splines, both for steel and concrete, is proposed. These functions appear to be adequate in reproducing rapidly varying fields, like the stress gradients occurring in the shear lag problem near the boundaries or where slips and/or cracks occur. Their use allow to use few macro-element instead of the very dense meshing required in those areas by the traditional FE interpolations.

Keywords Bond-slip analysis · Fracture in concrete · Strong discontinuity · Bezier interpolation

L. Contrafatto · M. Cuomo (✉) · F. Fazio
Department of Civil and Environmental Engineering, University of Catania, Catania, Italy
e-mail: massimo.cuomo@dica.unict.it

L. Contrafatto
e-mail: loredana.contrafatto@dica.unict.it

1 Introduction

In composite structural systems whose matrix exhibits a brittle behaviour, cracks in the matrix, inclusions and slip between the phases cause large stress gradients, so that it is necessary to model, in addition to the usual dissipative phenomena, also discontinuities in the displacement (strong) or in the deformation (weak) fields. Many structural systems fall within this description; among them, composites with brittle matrix, fibre reinforced and steel reinforced concrete structures, laminated structural glass etc. Slip between the phases plays an important role, in the sense that it determines the stress transfer rate, and thus introduces gradients in the stress field that allow to localise the crack positions. Slip can be considered to occur in a zero thickness interface, so that it can be evaluated by means of a generalised Newmark model (Newmark et al. 1951). Since a specific constitutive assumption is introduced for the interface, the kinematic fields of the matrix and of the fibres turn out to be different. The model has been widely used for analysing composite elements, and particularly steel–concrete interactions (see for instance Lachner and Mang 2003).

The possibility of accounting for slippage at the fibres boundaries or at the interface has been explicitly addressed in several models that try to analyse the fibre composite material using homogenization techniques. Usually specific micro-mechanical models are employed, that require very fine meshes and averaging procedures. In the case of thin fibres, some approximations are possible. Very often the fibre is considered rigid and only the slippage is accounted for. Stress concentration arises at the tip of the fibre, so that a deformable interlayer is required in order to regularise the numerical solution (Liao and Reifsnider 2000; Chudoba et al. 2009). However, fibre deformation cannot be disregarded for long and medium fibres, like in the case of rebars in reinforced concrete.

An alternative common approximation is to simplify the slip-bond law, disregarding the elastic-like part and considering only the permanent slip as a discontinuity in the displacement field. Radtke et al. (2011) have considered tunnel-like discontinuities at the fibre boundary, that can degenerate into singular jumps in the case the thickness of the fibre tends to zero. They adopted the methodology introduced by the strong discontinuity approach (SDA) (Simo et al. 1993; Oliver 1996; Oliver et al. 1999; Linder and Armero 2007) accounting for the boundary traction. Oliver adopted a similar approach for steel fibres reinforced concrete, although the slip was included in the steel constitutive equation, modifying the plastic softening modulus (Oliver et al. 2008).

In the paper, fracture is modeled adopting the cohesive model, originally developed by Dugdale (1960), for ductile fracture, and Barenblatt (1962), for brittle fracture. An adequate traction-separation law is assumed in the process zone, following one of the many proposals existing in the literature for concrete.

In a finite element (FE) context, tracking of interfaces is a demanding task, since a necessary requirement for the well-posedness of the discretised problem is the C^0 continuity of the interpolation. Indeed, the simplest way for introducing interfaces is to use zero thickness elements between standard elements (Ortiz et al. 1987). The crack path is thus constrained to develop on prescribed positions, and this causes very large errors on the evaluation of the fracture energy dissipated, requiring either continuous remeshing or a very fine mesh in the zone where crack is likely to develop. In addition, potential interfaces are inserted among all the elements where the crack can propagate, increasing the number of degrees of freedom, and, since it is necessary to introduce a fictitious elastic deformation of the interface, this artificially increases the compliance of the structure. Strategies have been proposed for inserting interfaces only where needed, but then it is necessary to use some recovery procedure for projecting the stresses on the nodes (Caballero et al. 2007; Ciancio et al. 2007).

Alternative to interelement interfaces are the strategies that employ intraelement interfaces, either increasing the nodal degrees of freedom or introducing appropriate enhancements in the displacement or deformation fields. XFEM, based on extra nodal degrees of freedom, has been largely employed in the simulation of propagating fractures (see, for instance, Moës et al. 1999; Belytschko et al. 2001). In the paper the element with embedded discontinuities (EED) formulation is adopted, (Simo and Oliver 1994; Jirásek and Zimmermann 2001; Mosler 2005; Oliver et al. 2006; Alfaiate et al. 2003), whose main advantage is that the additional degrees of freedom can be condensed at the element level. However, treating the additional degrees of freedom related to the enhancement as global, it is possible to guarantee the continuity of the discontinuity, as in Dias-da Costa et al. (2009, 2010). It is noted that XFEM presents a discontinuous gradient on either side of the interface, contrarily to EED, at least in the case of its classical implementation with constat jump.

Somewhat intermediate between the two previously described methods are the formulations based on discontinuous Galerkin (DG) approximations. This method uses discontinuous piecewise polynomial interpolations and allows for the use of unstructured meshes, while the continuity conditions are variationally imposed on the boundaries of the elements. DG methods are, thus, ideal in the case that a cohesive interface has to be modeled, and have been used both for static fracture (Prechtel et al. 2011) and for dynamic fracture (Huang and Costanzo 2004). DG have also been used for simulating fracture processes in structural models, like shells and beams. In the latter case, it was considered an homogeneous brittle beam, and a cohesive law was suggested to apply directly to the stress resultants in terms of the dual openings (Becker and Noels 2011). DG methods, so far, have not been applied to the case of reinforced concrete beams.

In Ibrahimbegovic et al. (2010) an approach based on EED and XFEM is used for modeling the final crack-spacing and opening in reinforced-concrete (RC)

structures, accounting for non linear concrete, steel and bond-slip constitutive models. In De Luycker et al. (2011) the XFEM formulation is incorporated into isogeometric analysis to obtain solutions with higher order convergence rates for problems in linear fracture mechanics. In comparison with XFEM with conventional FEs of equal degree, the NURBS-based isogeometric analysis gave equal asymptotic convergence rates and equal accuracy with fewer degrees of freedom (DOF). Isogeometric interpolation is becoming a widely employed paradigm for FE analysis (see for instance Auricchio et al. 2007; Kiendl et al. 2009; Benson et al. 2011; Borden et al. 2011). Verhoosel et al. (2011) used isogeometric FEs for discretising the cohesive zone formulation for failure in materials. They proposed a method based on discontinuous splines created by means of the knot-insertion technique. They found that T-splines are able to reproduce the crack path. The method has also been employed for the analysis of prestressed box-girder bridges in Choi et al. (2002) using the finite strip method (FSM), where isoparametric non-periodic B3-spline are introduced to simulate the displacement Kronecker delta property at the mid-span support of multispan bridge.

All the methods mentioned avoid the need of remeshing. In brittle homogeneous structures under a uniform strain field, it is not possible to localise the position of the fracture. This can be a serious problem in slender structures mainly subjected to bending, where the distance of successive cracks is strongly influenced by the interaction between the matrix and the reinforcement (Oliver et al. 2008). Moreover, in very thin plates subjected to bending, like in the case of laminated glasses, the interaction with the interlayer is essential for correctly predicting the crack pattern. In these cases, it appears essential to employ a non-homogeneous model.

In the paper we study the behaviour of reinforced concrete elements, including crack formation and concrete/steel slip. An elastic–plastic constitutive relation is used for the steel while the CEB-FIP proposal is adopted for the interface. Specifically, a one-dimensional element consisting in a beam with a single uniform reinforcement is considered.

The methodology proposed in the paper differs from the previous ones in two main points. First, different kinematic fields are considered for the matrix and the fibres. In this way, additional degrees of freedom are introduced, although they can be condensated using macro-elements. Crack opening in the matrix is introduced by means of a SDA. From the variational formulation of the enhanced problem all the relevant equations, including the interface equilibrium between the traction and the continuum stress, are derived. Two enhancements of the kinematics, based on polynomial or exponential shape functions respectively, are compared with the usual SDA enhancement. The matrix displacement field is assumed as the sum of a regular continuous field, related to the nodal degrees of freedom, plus a discontinuous field related to the displacement jump across the crack.

As an alternative approach, high-order interpolation based on B-splines is used. Both the concrete and the steel displacement fields are interpolated with B-splines. These functions appear to be adequate to interpolate displacement fields rapidly varying, and result quite stable in the numerical implementation.

The outline of the paper is the following. In Sect. 2 the ruling equations of the problem and the constitutive assumption are described. Section 3 contains the variational formulation and the FE implementation. In Sect. 4 polynomial and exponential shape function approximations are considered while in Sect. 5 the case of B-splines is examined. Finally, in Sect. 6.1 numerical applications and comparisons are illustrated. The advantages of the latter formulation on the previous are discussed. Some conclusions close the paper.

2 Bar slip in reinforced concrete under uniaxial regime

It is examined the case of a concrete beam in which a single reinforcement bar occupies the centroidal position. The unit is subjected to an uniaxial stretch. Let L be the length of the beam. The adopted model considers two separate phases (concrete–steel) joined by a deformable interphase of zero thickness. Each phase, as well as the interphase, is characterised by their own constitutive behaviour. The degrees of freedom of the system are the displacements of steel and concrete, $u_s(x)$ and $u_c(x)$, respectively. The corresponding infinitesimal axial deformations are given by

$$\varepsilon_s = \frac{\partial u_s}{\partial x}, \quad \varepsilon_c = \frac{\partial u_c}{\partial x} \tag{1}$$

and the slip is given by $\Gamma = \gamma t = u_s - u_c$, γ being the shear strain at the material interface and t the thickness of the beam. The conjugate dual variables are σ_s,

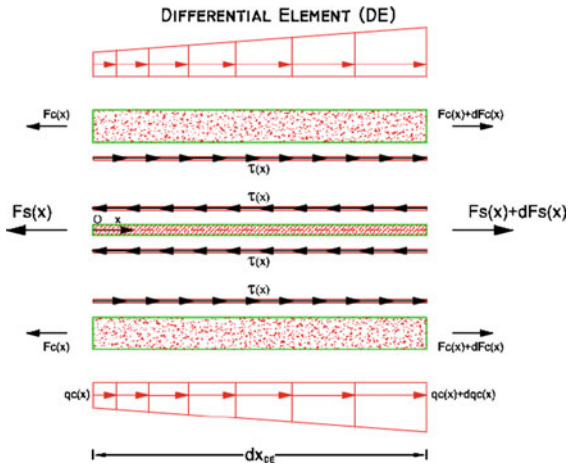

Fig. 1 Forces acting on a typical element

σ_c, τ. Therefore the virtual work identity can be written in the form:

$$\int_0^L A_s \sigma_s \tilde{\varepsilon}_s dx + \int_0^L A_c \sigma_c \tilde{\varepsilon}_c dx + \int_0^L C_s \tau(\tilde{u}_s - \tilde{u}_c) dx = [F_s \tilde{u}_s + F_c \tilde{u}_c]_0^L \tag{2}$$

where A_s and A_c are respectively the cross-sectional areas of the steel bar and of the concrete, while $C_s = \pi D_s$ is the rebar perimeter, D_s being the diameter.

Figure 1 shows the stresses acting on the elements. The model has been widely used both for reinforced concrete structures and for delamination problems since it was proposed by Newmark et al. (1951) for steel–concrete composite structures. In the case all the phases behave linearly with elastic moduli E_s, E_c, G_0, it is very easy to obtain a closed form solution of the equilibrium equations derived form the identity (2):

$$\begin{aligned} A_s E_s u_s'' - C_s G_0 (u_s - u_c) &= 0 \\ A_c E_c u_c'' + C_s G_0 (u_s - u_c) &= 0. \end{aligned} \tag{3}$$

The solution of the homogeneous equations are given by the vectors:

$$\begin{aligned} u_s &= \{Q_1 e^{\alpha x}, Q_1 e^{-\alpha x}, x, 1\} \\ u_c &= \{Q_2 e^{\alpha x}, Q_2 e^{-\alpha x}, x, 1\} \\ Q_1 &= \frac{1 + \frac{H}{\alpha^2}}{2} \\ Q_2 &= \frac{1 - \frac{H}{\alpha^2}}{2} \\ H &= C_s G_0 \left(\frac{1}{E_s A_s} - \frac{1}{E_c A_c} \right) \end{aligned} \tag{4}$$

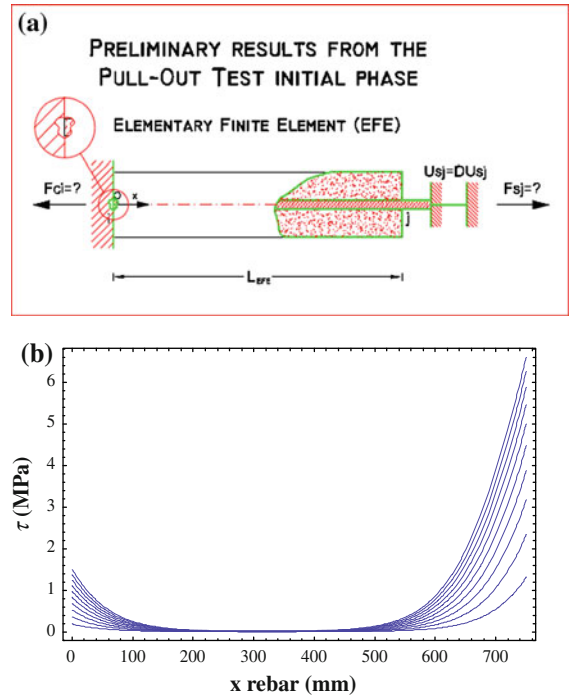

Fig. 2 Pull out test: **a** model. **b** Tangential slip stress

$$\alpha = \sqrt{C_s G_0 \left(\frac{1}{E_s A_s} + \frac{1}{E_c A_c} \right)}$$

A typical solution for the distribution of the tangential slip stresses τ at various levels of loading in a pull out test is shown in Fig. 2. The concrete core is constrained at the left end and free at the right one, while the rebar is free at both ends and an increasing displacement is applied on the right side. Large stress gradients occur at the right end of the bar, while the central zone undergoes a much more regular stress field. Therefore, in FE approximations of the problem, it is necessary that the mesh be quite refined in the region of large gradients. Moreover, when a crack occurs in the concrete, the stress fields exhibit analogous large gradients near the section of discontinuity, so that a fine mesh should be adopted since the start of the analysis, or a substantial mesh refinement is required in order to reduce the error.

Motivated by these considerations, in the paper the use of a different interpolation basis is proposed; particularly the performance of an exponential interpolation and of an interpolation based on B-splines will be examined. The latter appears to be a general tool that can be effectively extended to solid 2D and

3D elements exhibiting discontinuities on the displacement fields. The proposed interpolations will be compared with the standard FE approximation.

2.1 Constitutive assumptions

The constitutive behaviour of the materials is ruled by their elastic and inelastic potentials, denoted by φ, d, respectively. In the following, the equations will be defined, as usual, by means of the conjugated potentials φ^c, d^c.

The steel is supposed to behave elastoplastically with hardening. The elastic range is ruled by the complementary potential $\varphi_s^c = \frac{1}{2} E_s^{-1} \sigma_s \cdot \sigma_s$, while the complementary plastic potential is the indicator function of the set:

$$d_s^c = \mathrm{ind} K_s \qquad K_s = \left\{ (\sigma_s, \chi_s) : \sqrt{\sigma_s^2} - f_y - \chi_s \leq 0 \right\} \tag{5}$$

Either positive or zero hardening is considered. In the former case a linear isotropic hardening potential is assumed, $\psi_s^c = \frac{1}{2} H_s^{-1} \chi_s^2$, H_s being the steel hardening modulus.

In order to simplify the exposition, in what follows concrete will be assumed to behave linearly according to the elastic potential $\phi_c^c = \frac{1}{2} E_c^{-1} \sigma_c \cdot \sigma_c$. The hypothesis is anyhow not particularly restrictive as concrete is essentially in tension, until fracture opening occurs.

For the steel–concrete interface model the tangential stress τ due to slip is ruled by the CEB-FIP Model Code 90 (1993) in which a slight modification is introduced in the initial stiffness, in order to avoid a stick region that does not seem to be realistic. The assumed law is illustrated in Fig. 3, from which the meaning of parameters τ_{max} and Γ_1 can be inferred. The expression for the first branch is:

$$\tau(\Gamma) = \tau_{max} \frac{Log(1 + 4\tau_{max}\Gamma)}{Log(1 + 4\tau_{max}\Gamma_1)} \tag{6}$$

The process is assumed to be fully dissipative, that is upon unload the slip remains constant.

Details about the behaviour of the interface and its dissipative mechanism are not essential for the present work. Therefore, in the following text the interface constitutive model will be denoted in a generic way as $\tau = \tau(\Gamma)$.

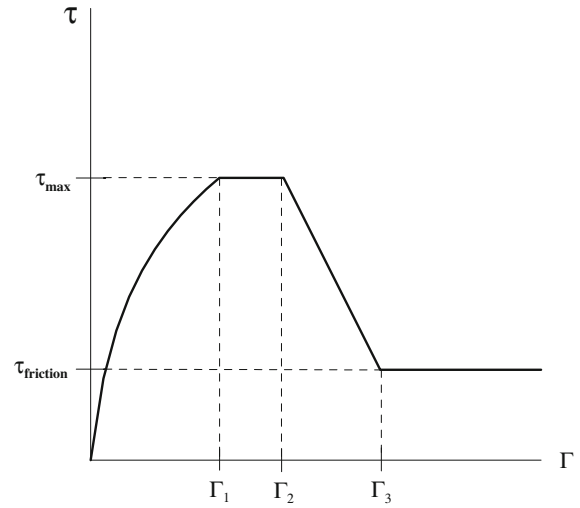

Fig. 3 CEB-FIP bond stress–slip relationship

2.2 Cohesive model of fracture

A fully dissipative cohesive model is used for concrete fracture, defined by the activation function:

$$g_n(t_n, \chi_n) = t_n - f_t^0 - \chi_n \leq 0 \tag{7}$$

In Eq. (7) t_n is the traction at the concrete interface, f_t^0 is the tensile resistance of concrete and χ_n rules the softening behaviour according to the potential Φ_n:

$$\chi_n = -\frac{\partial \Phi_n}{\alpha_{n_p}} \qquad H_n^t = \frac{\partial^2 \Phi_n}{\chi_n^2} \leq 0$$
$$\alpha_{n_p} = \alpha_{n_p}^0 + \lambda_n \frac{\partial g_n}{\partial \chi_n} \tag{8}$$

where α_{n_p} is the irreversible softening conjugated variable of χ_n and H_n the softening modulus. The potential Φ_n is such that

$$\int_0^\infty \chi_n d\alpha_{n_p} = G_f \tag{9}$$

G_f being the fracture energy of concrete.

The traction-opening displacement relation is given incrementally as:

$$\dot{w} = \frac{\partial d_n}{\partial t_n} = \lambda_n \frac{\partial g_n}{\partial t_n} = -\dot{\alpha}_{n_p} \tag{10}$$

3 Discontinuous model

We assume that a discontinuity has developed at a point x_c of the reinforced concrete element, and let w be the

actual value of the displacement jump. In general the intrinsic coordinate of the crack is known, and a non linear problem has to be solved in order to get its statical counterpart.

In this situation the displacement field in the concrete, and consequently the slip, are discontinuous.

The incremental problem is ruled by the mixed functional

$$\begin{aligned}\Pi = &\langle \sigma_s, \partial_x u_s \rangle - \langle \sigma_s, \varepsilon^0_{s_p} \rangle - \varphi^c_s(\sigma_s, \chi_s) \\ &- d^c_s(\sigma_s, \chi_s) - \langle \alpha^0_{s_p}, \chi_s \rangle + \langle \sigma_c, \partial_x u_c \rangle \\ &- \phi^c_c(\sigma_c) + \langle u_s - u_c, \tau \rangle - \langle \Gamma(\tau), \tau \rangle \\ &- \langle q_s, u_s \rangle - \langle q_c, u_c \rangle + [\Delta u_c(x_c), t_n] \\ &- \Phi^c_n(t_n, \chi_n) - [w^0_p, t_n] - d^c_n(t_n, \chi_n) \\ &- [\alpha^0_{n_p}, \chi_n]\end{aligned} \tag{11}$$

In formula (11) angular brackets indicate integration over the domain, while square brackets indicate integration over the cross-sectional area only. The subscript "n" denotes the potentials and the variables describing the interface behaviour of Sect. 2.2. α and χ are dual thermodynamical variables and q_s and q_c are the external loads.

The variation of (11) with respect to all the independent variables gives the relevant field equations of the slip problem:

$$\delta u_s \Rightarrow A_s \partial_x \sigma_s + C_s \tau - q_s = 0 \quad \text{in} \quad (0, L) \tag{12a}$$

$$\delta \hat{u}_c \Rightarrow A_c \partial_x \sigma_c - C_s \tau - q_c = 0 \quad \text{in} \quad (0, L) \tag{12b}$$

$$\delta \bar{u}_c \Rightarrow A_c \sigma_c = A_c t_n \quad \text{at} \quad x = x_c \tag{12c}$$

$$\delta \sigma_s \Rightarrow \partial_x u_s - \partial_{\sigma_s} \phi^c_s - \varepsilon^0_{s_p} - \partial_{\sigma_s} d^c_s = 0 \tag{12d}$$

$$\delta \chi_s \Rightarrow -\partial_{\chi_s} \phi^c_s - \alpha^0_{s_p} - \partial_{\chi_s} d^c_s = 0 \tag{12e}$$

$$\delta \sigma_c \Rightarrow \partial_x u_c - \partial_{\sigma_c} \phi^c_c \tag{12f}$$

$$\delta \tau \Rightarrow (u_s - u_c) - \Gamma(\tau) = 0 \tag{12g}$$

$$\delta t_n \Rightarrow w - w^0_p - \partial_{t_n} d^c_n = 0 \tag{12h}$$

$$\delta \chi_n \Rightarrow -H_n^{-1} \chi_n - \alpha^0_{n_p} - \partial_{\chi_n} d^c_n = 0 \tag{12i}$$

The set of equations (12) completely determines the solution of the problem.

Let us consider a FE discretization of the model in *nelem* elements of length L_e, whose elemental degree of freedom are the axial nodal displacements of the steel bar and of the concrete envelope, collected in the vector $\mathbf{d}^e$.

According to the Element Embedded Discontinuity method proposed by Simo et al. (1993), Simo and Oliver (1994), the displacement field in the concrete is assumed in the form:

$$u_c = \hat{u}_c + \bar{u}_c$$

$$\hat{u}_c = \sum_i N_{c_i} d^e_i \qquad \bar{u}_c = \bar{N}_c w = \left(H_{x_c} - \sum_{i \in \Omega^+} N_{c_i} \right) w \tag{13}$$

while for the displacement field of the rebar is used the standard approximation:

$$u_s = \sum_i N_{s_i} d^e_i \tag{14}$$

In Eqs. (13), (14) N_{c_i} and N_{s_i} are suitable shape functions and H_{x_c} is the Heaviside function at the point x_c. $\bar{N}_c$ depends on the interpolation functions relative to nodes in the region of the element Ω^+ beyond the discontinuity.

Therefore, in compact form, the following discretization define the FE model:

$$\begin{array}{lll} u_s = \mathbf{N}_s \mathbf{d}^e & \varepsilon_s = \mathbf{B}_s \mathbf{d}^e & \mathbf{B}_s = \frac{d}{dx} \mathbf{N}_s \\ u_c = \mathbf{N}_c \mathbf{d}^e + \bar{\mathbf{N}}_c w & \varepsilon_c = \mathbf{B}_c \mathbf{d}^e + \bar{\mathbf{B}}_c w & \mathbf{B}_c = \frac{d}{dx} \mathbf{N}_c \\ & \Gamma = \mathbf{B}_g \mathbf{d}^e + \bar{\mathbf{B}}_g w & \mathbf{B}_g = \mathbf{N}_s - \mathbf{N}_c \\ & & \bar{\mathbf{B}}_g = -\bar{\mathbf{N}}_c \end{array} \tag{15}$$

where $\mathbf{N}_s, \mathbf{N}_c$ are the matrices of steel and concrete shape function, $\mathbf{B}_s, \mathbf{B}_c$ contains their derivatives and $\bar{\mathbf{N}}_c$ is defined by Eq. (13). The shape functions for steel and concrete can be coincident or not, depending on the type of the adopted interpolation.

Let $\mathbf{d}$ be the global displacement vector and A the assembly operator. By introducing in (12) the usual Lagrangian regularization for the complementary dissipation potentials (Eve et al. 1990; Rockafellar 1970) and the approximation (15) the discrete field equations take the forms:

$$\delta \mathbf{d} \Rightarrow \mathop{A}_{e=1}^{nelem} \int_0^{L_e} \left(A_s \mathbf{B}_s^T \sigma_s + A_c \mathbf{B}_c^T \sigma_c + C_s \mathbf{B}_g^T \tau \right) dx - \mathbf{f}_{ext} = 0 \tag{16a}$$

$$\delta \mathbf{w} \Rightarrow \mathop{A}_{e=1}^{nelem} \int_0^{L_e} \left(A_c \bar{\mathbf{B}}_c^T \sigma_c + C_s \bar{\mathbf{B}}_g^T \tau \right) dx + A_c \mathbf{t}_n = 0 \tag{16b}$$

$$\delta \sigma_s \Rightarrow \mathbf{B}_s \mathbf{d}^e - E_s^{-1} \sigma_s - \varepsilon^0_{s_p} - \lambda_s = 0 \tag{16c}$$

$$\delta \chi_s \Rightarrow -H^{t^{-1}} \chi_s - \alpha^0_{s_p} + \lambda_s = 0 \tag{16d}$$

$$\delta \lambda_s \Rightarrow -\sigma_s + f_y + \chi_s = 0 \tag{16e}$$

$$\delta\tau \Rightarrow \mathbf{B}_g\mathbf{d}^e + \bar{\mathbf{B}}_g w - G_0^{-1}\tau - \Gamma_p^0 - \lambda_g = 0 \quad (16f)$$

$$\delta\chi_g \Rightarrow -\frac{\partial\phi_g^c}{\partial\chi_g} - \alpha_{g_p}^0 + \lambda_g = 0 \quad (16g)$$

$$\delta\lambda_g \Rightarrow -\tau + \tau_{max} + \chi_g = 0 \quad (16h)$$

$$\delta\sigma_c \Rightarrow \mathbf{B}_c\mathbf{d}^e + \bar{\mathbf{B}}_c w - E_c^{-1}\sigma_c = 0 \quad (16i)$$

$$\delta t_n \Rightarrow w - w_p^0 - \lambda_n = 0 \quad (16j)$$

$$\delta\chi_n \Rightarrow -H^{-1}t_n - \alpha_{n_p}^0 + \lambda_n = 0 \quad (16k)$$

$$\delta\lambda_n \Rightarrow -t_n + f_t^0 + \chi_n = 0 \quad (16l)$$

The variables of the problem can be grouped in global (the displacements **d** and the jumps **w**) and local (all the others), that are evaluated at the integration points of the element. The jump **w**, in the usual strong discontinuity framework, is condensed at local level; therefore it is evaluated together with the history constitutive variables in the local iteration. However, in a general approach, the points at which the discontinuities are evaluated could be taken on the elements boundary (in order to guarantee continuity of the displacement field); in this case the jumps are treated as global variables. This strategy has been used in Ayala et al. (2010), Dias-da Costa et al. (2009). It presents general computational advantages, some of which will appear from the following developments, and it will be adopted in this paper.

3.1 Solution strategy

At each step it is required to find a solution of the non linear equilibrium equations

$$\overset{nelem}{\underset{e=1}{A}} \sum_{i\in GP} \left[\left(A_s\mathbf{B}_s^T(\xi_i)\sigma_{s_i} + A_c\mathbf{B}_c^T(\xi_i)\sigma_{c_i} + C_s\mathbf{B}_g^T(\xi_i)\tau_i\right) w_i^{GP}\right] - \mathbf{f}_{ext} = \mathbf{r}_d \quad (17)$$

$$\overset{nelem}{\underset{e=1}{A}} \sum_{i\in GP} \left[\left(A_c\bar{\mathbf{B}}_c^T(\xi_i)\sigma_{c_i} + \bar{\mathbf{B}}_g^T(\xi_i)C_s\tau_i\right) w_i^{GP}\right] + A_c\mathbf{t}_n = \mathbf{r}_w \quad (18)$$

where GP is the set of the integration points located at some natural abscissa ξ_i, and w_i^{GP} are the corresponding weights. The residual method requires that the residuals be driven to zero by means of the iterative solution of the first order expansion

$$\begin{bmatrix} \mathbf{K}_{dd} & \mathbf{K}_{dw} \\ \mathbf{K}_{wd} & \mathbf{K}_{ww} \end{bmatrix} \begin{bmatrix} \mathbf{d} \\ \mathbf{w} \end{bmatrix} = \begin{bmatrix} -\mathbf{r}_d \\ -\mathbf{r}_w \end{bmatrix} \quad (19)$$

where

$$\mathbf{K}_{dd} = \overset{nelem}{\underset{e=1}{A}} \sum_{i\in GP} \left[\left(A_s\mathbf{B}_s^T(\xi_i)E_s^t(\xi_i)\mathbf{B}_s(\xi_i) + A_c\mathbf{B}_c^T(\xi_i) \times E_c^t(\xi_i)\mathbf{B}_c(\xi_i) + C_s\mathbf{B}_g^T(\xi_i)G^t(\xi_i)\mathbf{B}_g(\xi_i)\right) w_i^{GP}\right] \quad (20)$$

$$\mathbf{K}_{dw} = \overset{nelem}{\underset{e=1}{A}} \sum_{i\in GP} \left[\left(A_c\mathbf{B}_c^T(\xi_i)E_c^t(\xi_i)\bar{\mathbf{B}}_c(\xi_i) + C_s\mathbf{B}_g^T(\xi_i)G^t(\xi_i)\bar{\mathbf{B}}_g(\xi_i)\right) w_i^{GP}\right] \quad (21)$$

$$\mathbf{K}_{ww} = \overset{nelem}{\underset{e=1}{A}} \sum_{i\in GP} \left[\left(A_c\bar{\mathbf{B}}_c^T(\xi_i)E_c^t(\xi_i)\bar{\mathbf{B}}_c(\xi_i) + C_s\bar{\mathbf{B}}_g^T(\xi_i)G^t(\xi_i)\bar{\mathbf{B}}_g(\xi_i)\right) w_i^{GP}\right] + K_n^t A_c \quad (22)$$

The value of the interface traction $\mathbf{t}_n$ needed for the residual calculation and the algorithmic tangent moduli are obtained from the solution of the non linear constitutive equations at the i-th Gauss point, that, in the strategy adopted, are totally uncoupled, since the only coupling equation, i.e., the equilibrium on the discontinuity surface, has been added to the global iteration. Therefore, at each Gauss point, the stress in the constituents and in the steel–concrete interface and the algorithmic tangent moduli stem from the following systems of equations:

$$\begin{bmatrix} E_s^{-1} & 0 & 1 \\ 0 & H^{-1} & -1 \\ 1 & -1 & 0 \end{bmatrix} \begin{bmatrix} \sigma_{s_i} \\ \chi_{s_i} \\ \lambda_{s_i} \end{bmatrix} = \begin{bmatrix} \mathbf{B}_s(\xi_i)\mathbf{d}^e - \varepsilon_{s_{p_i}}^0 \\ -\alpha_{s_{p_i}}^0 \\ f_y \end{bmatrix} \quad (23)$$

$$E_c^{-1}\sigma_{c_i} = \mathbf{B}_c(\xi_i)\mathbf{d}^e + \bar{\mathbf{B}}_c(\xi_i)w \quad (24)$$

$$\begin{bmatrix} G_0^{-1} & 0 & 1 \\ 0 & \frac{\partial^2\phi_g^c}{\partial\chi_g}^2 & -1 \\ 1 & -1 & 0 \end{bmatrix} \begin{bmatrix} \tau_i \\ \chi_{gi} \\ \lambda_{gi} \end{bmatrix} = \begin{bmatrix} \mathbf{B}_g(\xi_i)\mathbf{d} + \bar{\mathbf{B}}_g(\xi_i)w - \Gamma_{p_i}^0 \\ -\alpha_{g_{p_i}}^0 \\ \tau_{max} \end{bmatrix} \quad (25)$$

$$\begin{bmatrix} 0 & 0 & 1 \\ 0 & H_n^{t\,-1} & -1 \\ 1 & -1 & 0 \end{bmatrix} \begin{bmatrix} t_n \\ \chi_n \\ \lambda_n \end{bmatrix} = \begin{bmatrix} w - w_p^0 \\ -\alpha_{p_n}^0 \\ f_t^0 \end{bmatrix} \quad (26)$$

Specifically, the last system yields the tangent softening modulus K_n^t.

4 Polynomial and exponential shape functions

The procedure outlined in the previous section applies to different choices of the interpolation functions. First we consider a beam element with four degrees of freedom ($\mathbf{d}^e = \{d_{1_s}, d_{1_c}, d_{2_s}, d_{2_c}\}$). Equation (15) define the discrete displacement field. Two cases are examined. In the first one the usual polynomial shape functions are adopted (specifically linear in each element); in the second one shape functions derived from the basis (4) of the system of differential equations (3) is used (exponential shape functions).

The expressions of these shape functions as well as the related plots are reported in "Appendix A". These shape functions are problem oriented, in the sense that they depend on the geometrical and mechanical parameters of the element to which they apply, collected in the parameters α and H reported in the appendix.

Note that in the case of the exponential interpolation both the steel and the concrete displacement fields depend in general on all of the four nodal displacements, according to the solution of the equilibrium equations (4). The shape functions for the steel and the concrete are different, still respecting a partition of unity; in this way to each degree of freedom it is also associated the relevant slip.

The enhanced shape function $\bar{N}_c$, as indicated in expression (14), is obtained summing the two shape functions relative to one of the ends of the bar. The function so obtained is linear, thus it is the same as the enhanced shape function used with the linear interpolation. We therefore expect that some of the advantages of using exponential shape functions will be lost near the sections of discontinuity. This aspect will be discussed in the section dedicated to the numerical results.

We notice that the exponential shape functions are an exact solution of the linear shear lag equations; therefore, they give a variational solution when a non linear analysis is performed. A comparison of the solutions obtained using the two forms of interpolation is discussed in Sect. 6.1.

The stress concentration arising near the crack is better described using high order (exponential) shape functions, without having to introduce many tiny elements, most of them being subjected to almost constant stress state. However, significant errors on the equilibrium are evident at the boundary of the element.

5 An alternative enriched finite element for slip and crack

In this section we introduce an enriched FE able to account both for slip and crack opening in the concrete, that uses high order interpolation, and that can be easily adapted to the occurrence of discontinuities. As interpolation functions we propose to use B-splines. B-splines are families of piecewise functions defined in [0, 1] that constitute a partition of unity. The degree p of the B-spline is the polynomial degree. B-splines are defined on a knot vector, that is a sequence of $m + 1$ non decreasing values in the interval [0, 1], $\xi_k \in [0, 1]$, $k = 0, \ldots, m$. A B-spline curve is an interpolation obtained by

$$\mathbf{P}(\xi) = \sum_{i=0}^{n} b_{p,i}\mathbf{P}_i \tag{27}$$

where $\mathbf{P}_i$ are a set of $n+1$ control points and $b_{p,i}$ is the i-th B-spline of order p. If $n + 1$ is the number of control points the knot vector contains $p + (n + 1) + 1$

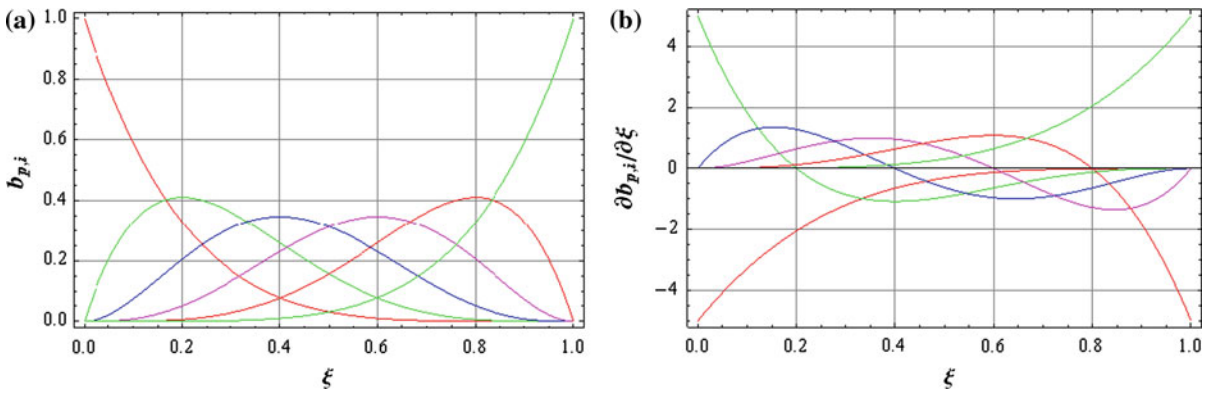

Fig. 4 Bernstein Polynomials of order 5 (**a**) and their derivatives (**b**)

knots. The interval between two subsequent knots $[\xi_k, \xi_{k+1}]$ is known as 'segment' (in the CAD literature it is often called 'element', but we discard the latter definition in order to avoid confusion), and contains at most $p+1$ non zero splines. Each spline $b_{p,k}$ is non zero in the interval $[\xi_k, \xi_{k+p+1}]$. Two subsequent basis splines meet with continuity C^{p-1} at the k-th knot. When multiple knots are introduced, the spline presents a discontinuity of the order of the multiplicity of the knot. Consequently, for open splines the first and the last knots, of abscissa 0, 1, must have a multiplicity equal to $p+1$. Considering an open spline with no internal knots, we have only one segment, and exactly $p+1$ control points associated to independent basis splines, called Bezier splines, that reduce to the Bernstein polynomials, which, as it is well known, are a basis of a linear space dense on C^0. B-splines are a generalisation of Bernstein polynomials, that share similar properties, and in addition have a local character.

Either Bezier or B-splines functions are not shape functions, but they allow to interpolate both the initial geometry and the displacement fields; in the case examined here, we have:

$$u_s = \sum_{i=0}^{n} N_i d_{s_i} \qquad \varepsilon_s = \sum_{i=0}^{n} B_i d_{s_i}$$

$$u_c = \hat{u}_c + \bar{u}_c = \sum_{i=0}^{n} N_i d_{c_i} + \bar{N} w \quad \varepsilon_c = \sum_{i=0}^{n} B_i d_{c_i} + \bar{B} w \tag{28}$$

$$\Gamma = \sum_{i=0}^{n} \left(b_{p,i}\right)\left(d_{s_i} - d_{c_i}\right)$$

$$N_i = b_{p,i} \qquad B_i = \frac{db_{p,i}}{dx} = p\left(b_{p-1,i-1} - b_{p-1,i}\right)$$

In (28) the DOF's d_i are not nodal displacement, but refer to the variation of the coordinates of the control points, that interpolate the difference from the current and the reference configurations. Figure 4 shows the interpolation functions and their derivatives in the case of Bernstein basis of order 5. The pictures highlights how the interpolation meets the goal of reproducing high gradients near the points of discontinuity.

When B-splines are used there are $2(n+1)$ degrees of freedom, plus the discontinuities. The integrations for the residuals and the tangent matrices involve $p+1$ functions in each segment. If Bernstein polynomials are used, the segment coincides with the beam element.

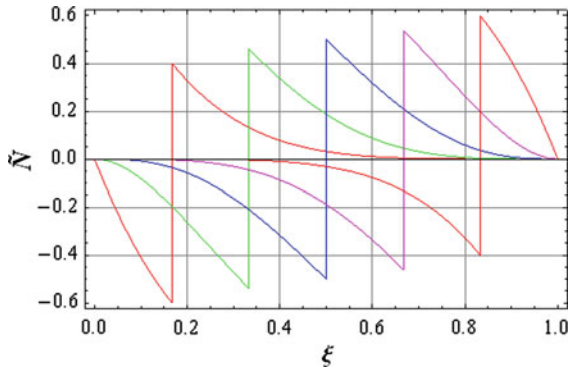

Fig. 5 Enhancement displacement function with unit jump for 5th order Bernstein Basis interpolation. Location of the discontinuity at {1/6, 2/6, 3/6, 4/6, 5/6}

In the latter case the enhanced shape function can be obtained as in the standard SDA, subtracting form the Heaviside function the sum of all the interpolation functions relative to nodes in region of the element Ω^+ that follows the location of the discontinuity.

$$\bar{N}_c = \left(H_{x_c} - \sum_{i \in \Omega^+} b_{p,i}\right) \tag{29}$$

In this way one single additional degree of freedom is associated to each discontinuity. Figure 5 represents the function $\bar{N}$ for several locations of the discontinuity along the bar. The method can be applied to the equations described in Sect. 2 without any major change, except the number of degrees of freedom per element and the scaling of the abscissa. The interpolation functions are of degree p, so that special integration rules have to be used. Since the functions have very high gradients near the ends of the element, Gauss–Lobatto quadrature is used, with $p+1$ integration points. This is necessary in order to guarantee a satisfactory evaluation of the matrices.

A quite different scheme is based on the use of B-splines, as suggested in Borden et al. (2011). In this case a discontinuity can be directly introduced in the interpolation by inserting an additional knot at the parametric abscissa corresponding to the point where the fracture has been detected, with multiplicity $p+1$. The number of control points then increases, as well as the number of segments that constitute the spline approximation. For instance, if an open B-spline without internal knots of order 5 had been used originally, with 6 control points, the insertion of an extra knot

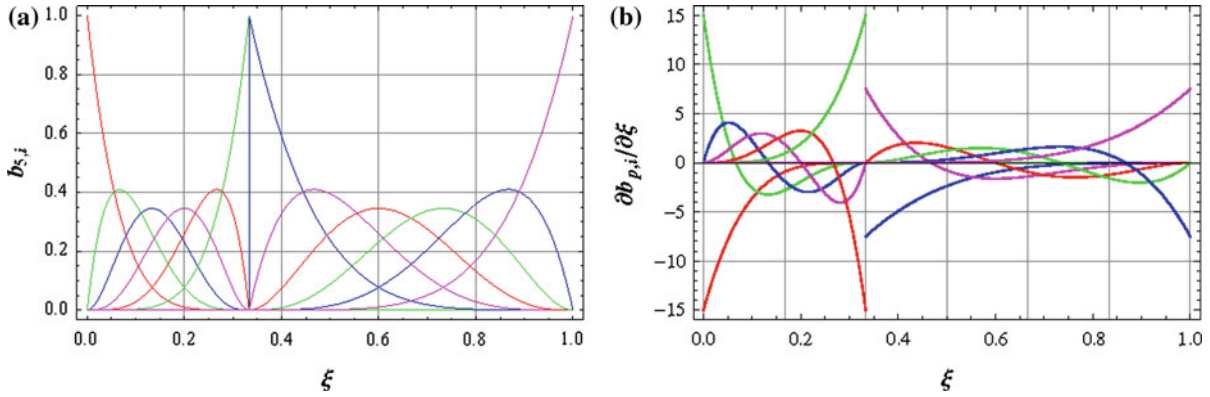

Fig. 6 B-splines of order 5 (**a**) and their derivatives (**b**) after a knot insertion of multiplicity 6 at $\xi = 1/3$

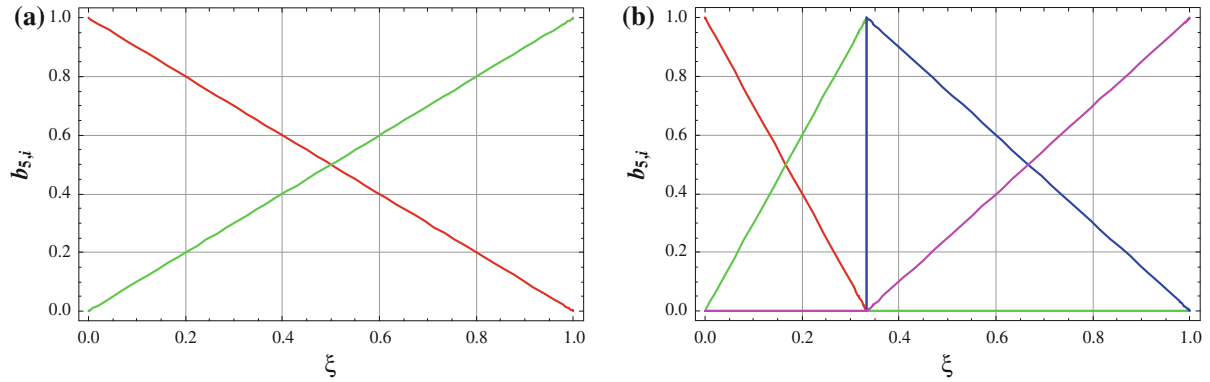

Fig. 7 Interpolation with B splines of degree 1: **a** without internal knots (knot vector = {1, 1, 0, 0}), **b** after the insertion of an internal knot at $\xi = 1/3$ (knot vector = {1, 1, 1/3, 1/3, 0, 0})

of multiplicity 6 leads to 12 control points, and the net effect is to split the original element into two, each one with a p-th order interpolation, as shown in Fig. 6, where are plotted also the derivatives of the functions. The method is thus quite different from the classical SDA, even though the additional degrees of freedom are still internal and can be treated as local. The main difference appears comparing the derivative of the function $\bar{\mathbf{N}}$ (Fig. 4) and the derivatives of the B-splines with additional knots (Fig. 6). The former is continuous and continuously differentiable, while the latter presents a discontinuity, so the stresses and strains can be different on both sides of the discontinuity surface. Although in the application presented in this work this property is unnecessary, it may be very useful in 2D and 3D applications, in order to avoid shear stress locking. In addition, multiple cracks in a single element can easily be handled by the method of knots insertion.

In order to get a better insight into the method, Fig. 7 shows an interpolation for a straight element based on the B-splines of order 1, that coincide with the usual linear shape functions, and the situation after the insertion of a knot of multiplicity 2 at the point of abscissa $\xi = 1/3$. The procedure is equivalent to subdividing the element into two, adding two new nodes, and the interface acts as a non linear spring between the two internal nodes.

In the case under examination, an initial interpolation of the whole uncracked beam is performed with uniformly spaced B-splines of order p without internal knots (Bezier curves), thus with $p + 1$ control points, both for the steel and the concrete displacements, and the first of the equilibrium equations (17) are solved. The use of uniform splines without internal knots has been found to yield a sufficient precision, minimising the computational cost. At each step the maximum stress in the concrete is evaluated with

a search algorithm. When it attains the limit tensile resistance, an internal knot with multiplicity $p+1$ is added to the knot vector for the concrete displacement interpolation, and new uniformly spaced control points are introduced in each of the segments generated on the beam. The coordinates of the new control points are evaluated interpolating the original Bezier interpolation, in order to be used as initial solution, i.e., calling $\mathbf{d}_i^{OLD} \quad i = 0, \dots p$ the coordinates of the control points prior to the knot insertion, and $\mathbf{d}_i^{NEW} \quad i = 0, \dots 2p+1$ the newly generated coordinates of the control points, for each segment of the beam it is solved the system:

$$\begin{bmatrix} b_{p,0}(0) & \dots & b_{p,p}(0) \\ b_{p,0}(1/p) & \dots & b_{p,p}(1/p) \\ \vdots & & \\ b_{p,0}(1) & \dots & b_{p,p}(1) \end{bmatrix} \begin{bmatrix} d_0^{NEW} \\ d_1^{NEW} \\ \vdots \\ d_p^{NEW} \end{bmatrix} = \begin{bmatrix} \sum_{i=0}^{p} b_{p,i}(0) d_i^{OLD} \\ \sum_{i=0}^{p} b_{p,i}(1/p) d_i^{OLD} \\ \vdots \\ \sum_{i=0}^{p} b_{p,i}(1) d_i^{OLD} \end{bmatrix} \tag{30}$$

The historical variables at the newly generated Gauss–Lobatto points are interpolated from those in the closest original locations of the Gauss points (except at the ends of the element, where the historical variables are directly transmitted to the new interpolation; notice that usually the most severe values of the historical variables occurs at the end points, so the error is minimised).

The steel displacements remain continuous, however, in order to keep a similar degree of approximation for both displacement fields, also the steel displacement interpolation is enhanced, introducing in the point where the crack has developed an internal knot of multiplicity smaller than $p+1$. Adding an internal knot with multiplicity $p-1$ guarantees continuity of the displacement and of the deformation field C^1 continuity), whether a knot with multiplicity p yields a C^0 continuity for the steel displacement field, and the deformation continuity is recovered variationally. The former case is illustrated in Fig. 8, and introduces $p-1$ additional control points. The latter case corresponds to split the beam into two elements enforcing the kinematic continuity on the steel degrees of freedom corresponding to the end points of the two elements.

Once the internal knot has been inserted, the relative displacement w is set equal to $d_{c,p+1} - d_{c,p}$, and the equilibrium equations are obtained from the variational principle (11), that for the DOF's d_{s_i}, d_{c_i} corresponding to a control point $\mathbf{P}_i, \quad i \neq \{p, p+1\}$ become

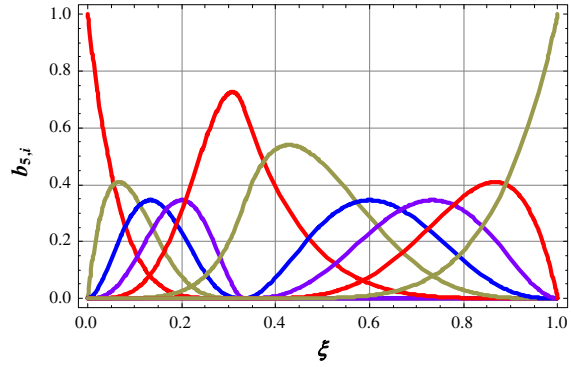

Fig. 8 Enhanced interpolation for the steel displacement with C^1 continuous B-splines of order 5 after a knot insertion of multiplicity 4 at $\xi = 1/3$, knot vector $\{0, 0, 0, 0, 0, 0, 1/3, 1/3, 1/3, 1/3, 1, 1, 1, 1, 1, 1\}$

$$\begin{aligned} &\sum_{k \in GP} \left[\left(A_s B_i(\xi_k) \sigma_{s,k} + C_s N_i(\xi_k) \tau_k \right) w_k^{GP} \right] \\ &- \mathbf{f}_{si}^{ext} = 0 \\ &\sum_{k \in GP} \left[\left(A_c B_i(\xi_k) \sigma_{c,k} - C_s N_i(\xi_k) \tau_k \right) w_k^{GP} \right] \\ &- \mathbf{f}_{ci}^{ext} = 0 \end{aligned} \tag{31}$$

while for the DOF's $d_{c,p}, d_{c,p+1}$ the equilibrium equations are

$$\begin{aligned} &\sum_{k \in GP} \left[\left(A_c B_p(\xi_k) \sigma_{c,k} - C_s N_p(\xi_k) \tau_k \right) w_k^{GP} \right] - A_c t_n = 0 \\ &\sum_{k \in GP} \left[\left(A_c B_{p+1}(\xi_k) \sigma_{c,k} - C_s N_{p+1}(\xi_k) \tau_k \right) w_k^{GP} \right] + A_c t_n = 0 \end{aligned} \tag{32}$$

The latter are the equilibrium equations at the interface, that involve the concrete stress and also the tangential stresses due to slip. The tangent stiffness operator is obtained from the solution of the local problem, that is analogous to the one described in Sect. 3.1. The integrals are performed numerically, using a Gauss–Lobatto quadrature. It can be shown that the order of quadrature must be at least equal to the degree of the splines plus one.

6 Numerical results

The model presented in Sect. 2 and the performance of the interpolations introduced in Sects. 4, 5 are discussed with the aim of the pull out example shown in

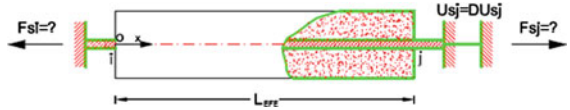

Fig. 9 Geometry of the pull out test simulated in Sect. 6.1. $L = 750\,\text{mm}$; steel bar diameter $D_S = 12\,\text{mm}$; concrete rod diameter $D_c = 90\,\text{mm}$

Fig. 9. The ratio $\mu = \frac{A_s}{A_c}$ denotes the geometrical percentage of steel. A class C25 concrete has been used, setting $f_{ck} = 22.95\,\text{MPa}$ for the compression strength, and $E_c = 29{,}000\,\text{MPa}$ for the elastic modulus. Its limit tensile resistance has been set equal to 2.42 MPa, fracture energy has been estimated according to usual rules as $G_f = 0.0662\,\text{N/mm}$. Linearly hardening steel has been assumed, with yield stress $\sigma_{sy} = 420\,\text{MPa}$, and plastic modulus $E_{sp} = 10{,}000\,\text{MPa}$. For the tangential stress–slip relationship the CEB-FIP rule has been used, with the parameters related to unconfined concrete, that is:

$$\begin{aligned} \tau_{max} &= 2.50\sqrt{f_{ck}} = 11.98\,\text{MPa} \\ \Gamma_1 &= 1.0\,\text{mm} \\ \Gamma_2 &= 3.0\,\text{mm} \\ \Gamma_3 &= 5.0\,\text{mm} \end{aligned}$$

The test is geometrically symmetric, so the first crack arises at the beam midpoint. First are examined the results obtained with the polynomial and the exponential interpolation, then those obtained with the B-spline interpolation.

6.1 Polynomial and exponential approximations

The simulation has been carried out until the first crack has developed. Figure 10 summarises the results obtained using the low order linear interpolation dividing the beam with a number of elements ranging from 3 to 15. In the pre-crack branch of the end force-displacement plot is apparent the non linearity due to the non linear constitutive relation used for the slip. The performance of the linear interpolation is quite poor, and convergence is very slow. Using few elements results in large errors, as expected.

The performance of the exponential interpolation is summarised in Fig. 11. The advantage of using a problem oriented interpolation is clearly shown by the very fast convergence of the simulation. Even the crack opening and the post-peak branch of the load curve are almost exactly estimated even with very few elements (Fig. 12). Comparing the stress along the steel bar predicted by the models at a sequence of steps of the simulation, the errors associated with the linear interpolation appear still greater (Fig. 13). The stress obtained with the exponential interpolation shows a C^1 continuity at the interface, due to the type of enhancement adopted. This seems an unnecessary limitation, especially for the stress in the concrete bar, that can be removed using the B-spline interpolation. Finally it is observed that equilibrium at the boundary of the elements is not exactly enforced, as usual in FE approximations.

6.2 B-splines approximations

The same test has been analysed with the B-spline interpolation. A linear approximation for the bond-slip constitutive relation has been employed in this case. Uniform splines of degree 5 have been used. The stresses diagrams of Fig. 14 show that the model is able to accurately predict the stress distribution, included the discontinuity on the slope of the steel stress. In Figs. 15, 16 is highlighted the influence on the crack formation of the percentage of the reinforcement area and of the fracture energy. The greater the fracture energy, the smoother is the post peak behaviour.

Figure 17 present the comparison of the results obtained with the present model and some experimental results of a pull out test (Keuser and Mehlhorn 1987). The data are the same used by Prasad and Krishnamoorthy (2002), that is $L = 500\,\text{mm}$, $D_s = 16\,\text{mm}$, $D_c = 150\,\text{mm}$. Steel is linearly hardening with $\sigma_{sy} = 353\,\text{MPa}$, $E_{sp} = 2{,}050\,\text{MPa}$, the elastic modulus of concrete is $E_c = 35{,}000\,\text{MPa}$, its compression and tensile strength have been set equal to $f_{ck} = 46.5\,\text{MPa}$, $f_{ct} = 2.7\,\text{MPa}$ and $G_f = 0.086\,\text{N/mm}$. In the plot is reported the stress in half of the steel bar at three stages of the test. The experimental results show that when the crack opens (40 KN) the stress in the steel bar is not symmetric. This result is correctly simulated if a cohesive law is used for the crack opening, where the value of the softening parameter is obtained from the fracture energy of concrete, while using lower values of the fracture energy (in the limit, zero), a symmetric stress distribution is obtained. When the steel bar plasticise (70 KN) the symmetry in the stress distribution is recovered.

Fig. 10 Pull-out test. End force versus bar displacement. Linear interpolation

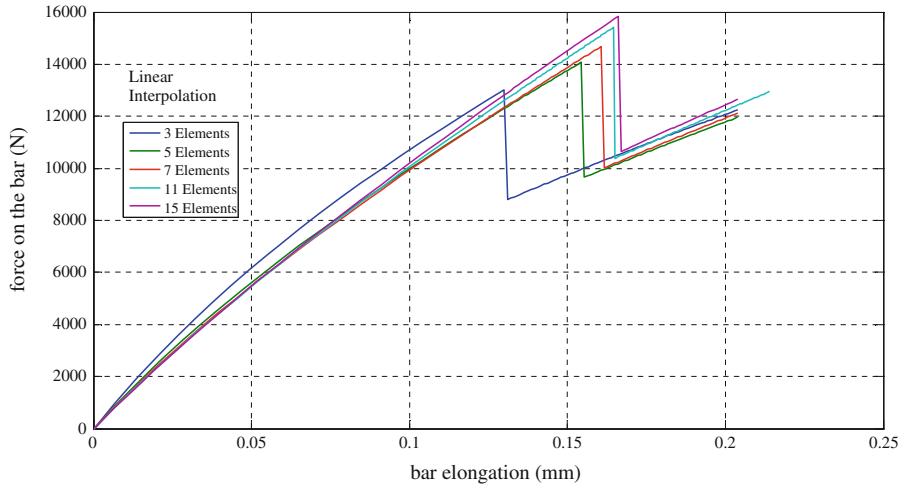

Fig. 11 Pull-out test. End force versus bar displacement. Exponential interpolation

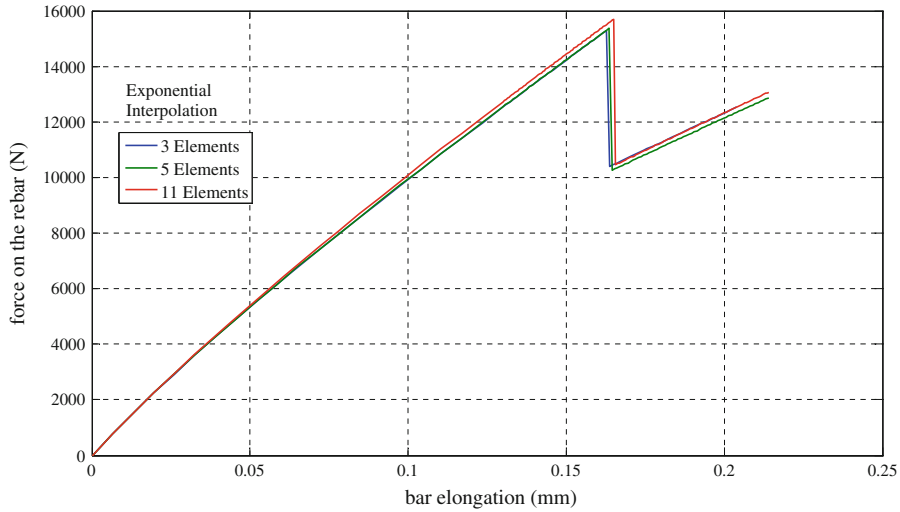

Fig. 12 Pull-out test. Crack opening versus bar displacement. Exponential interpolation

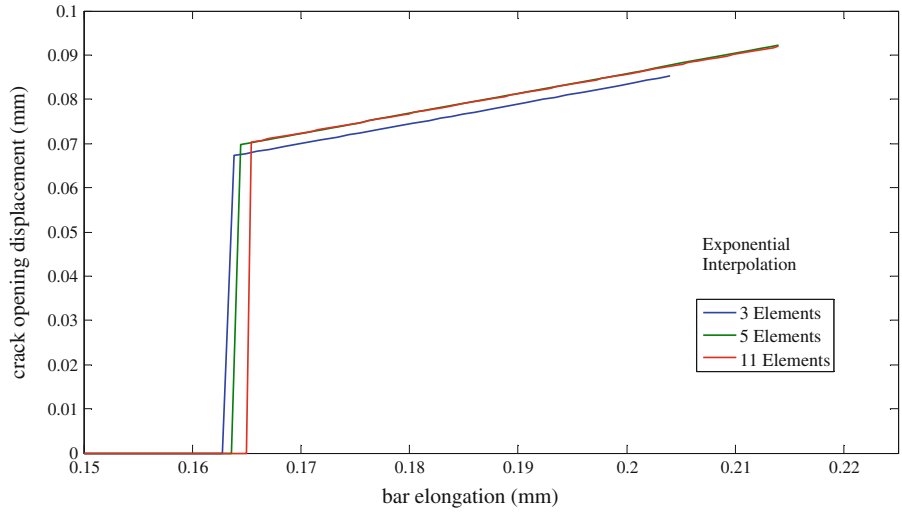

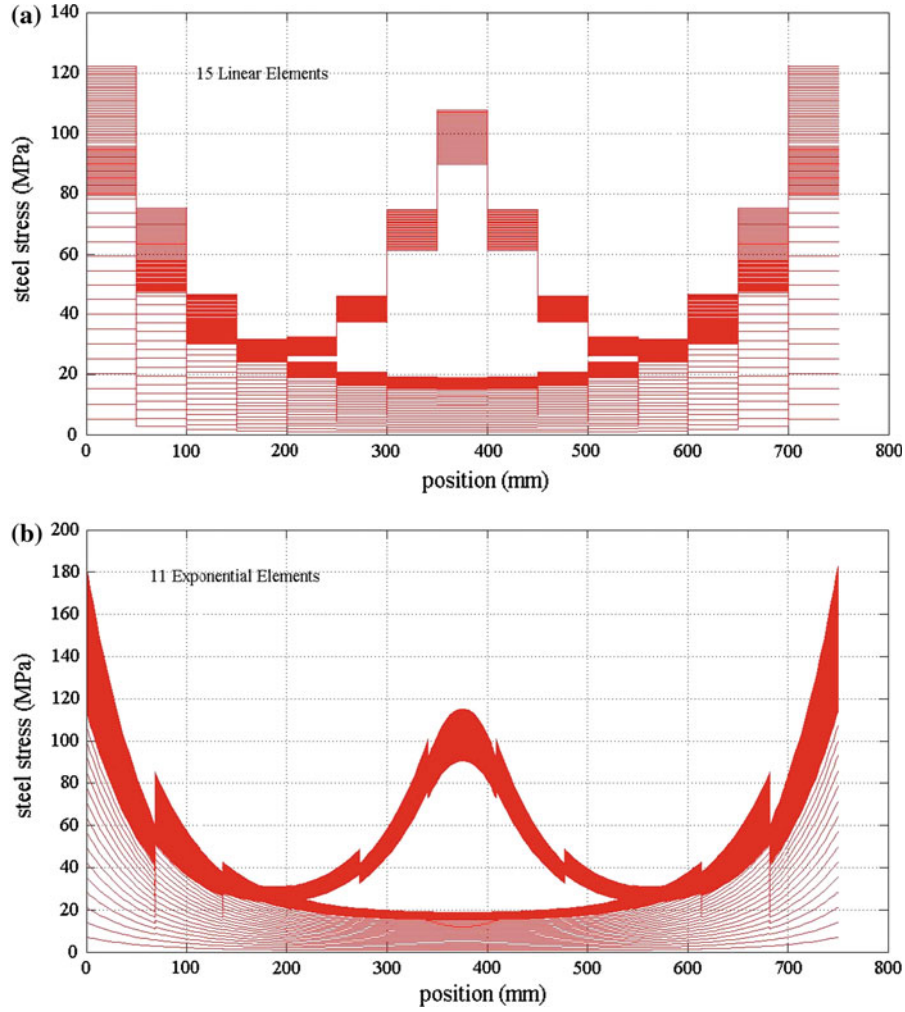

Fig. 13 Stress along the steel bar. Comparison between 15 linear elements (**a**) and 11 exponential elements (**b**)

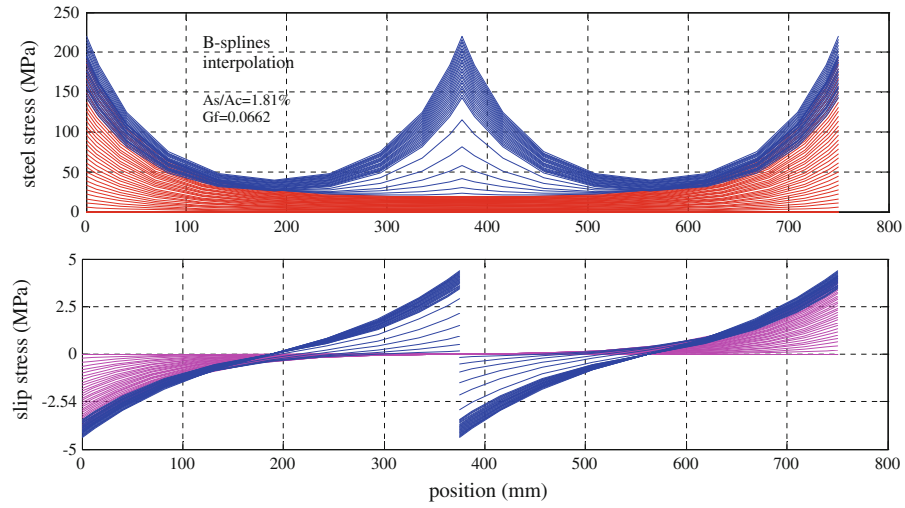

Fig. 14 Stresses along the steel bar and slip stresses. B-splines interpolation

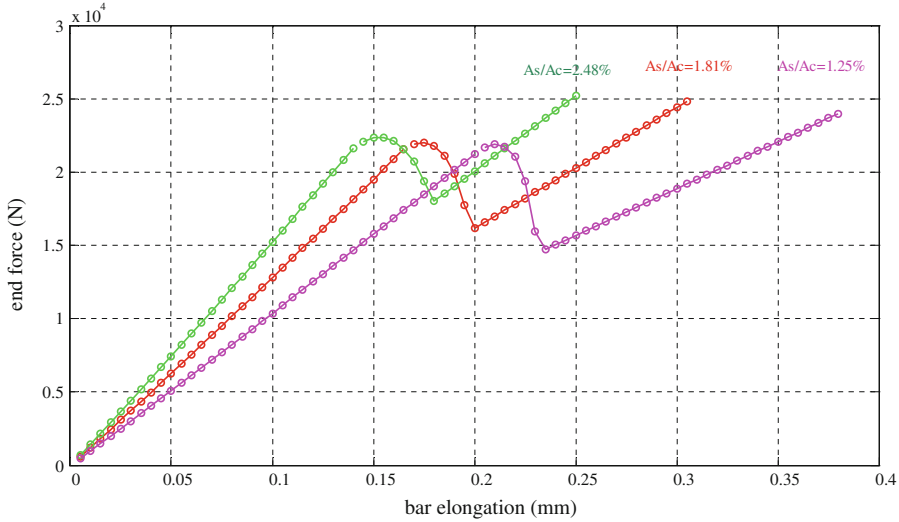

Fig. 15 Pull-out test on beams with different percentage of steel. B-splines interpolation

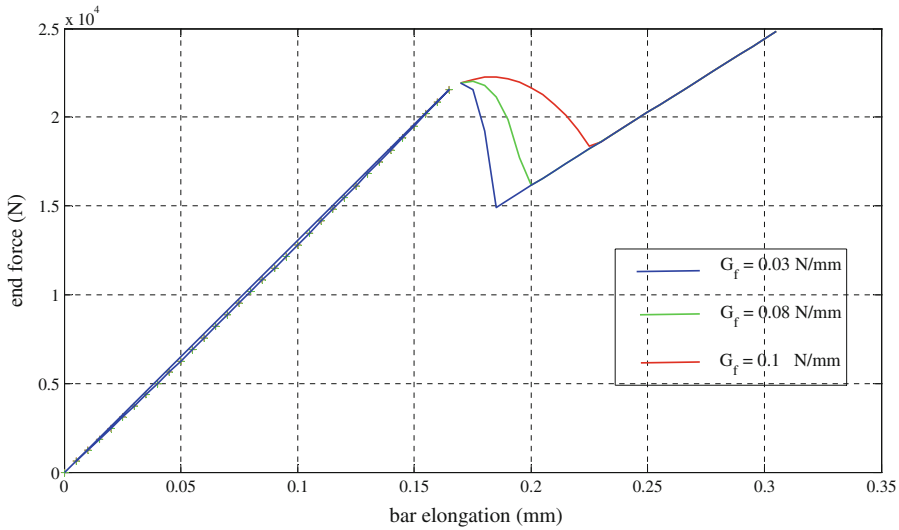

Fig. 16 Pull-out test on beams with different fracture energy. B-splines interpolation

7 Conclusions

It has been illustrated a FE implementation of the shear lag model for the analysis of a concrete bar accounting for steel–concrete slippage and for crack formation in the concrete. A complete variational formulation of the problem has been presented, of the Hesslinger Reissner type, that includes the duality pairings and the energy potential of the cracking interface.

It has been shown that low order elements as those commonly used in FE codes lead to large errors, due to the fact that the gradient of the stresses is very high near the extremities of the fibre and where a crack occurs. Since, generally, the position of the crack is not known a priori, it is necessary to use a very fine mesh, that for most of the model is, however, redundant. Therefore it has been proposed to use elements based on high order interpolations. Two alternative methods have been analysed. The first makes use of exponential shape functions, derived from the exact solution of the linearised shear lag equations. The shape functions carry the memory of the problem since they change according to the mechanical and geometrical properties of the element. These functions have been proved to be very effective. Although in the paper only the axial problem has been examined, it is very easy to extend the method to the bending behaviour of the beam. A drawback for this kind of interpolation is the treatment

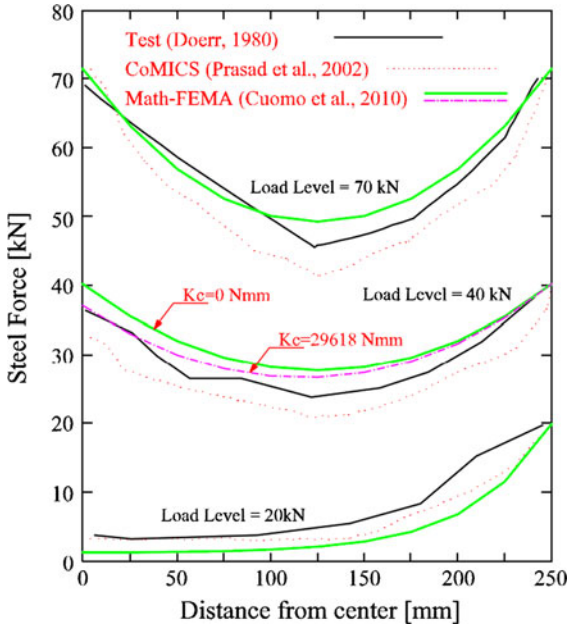

Fig. 17 Simulation of the pull out test reported in Prasad and Krishnamoorthy (2002)

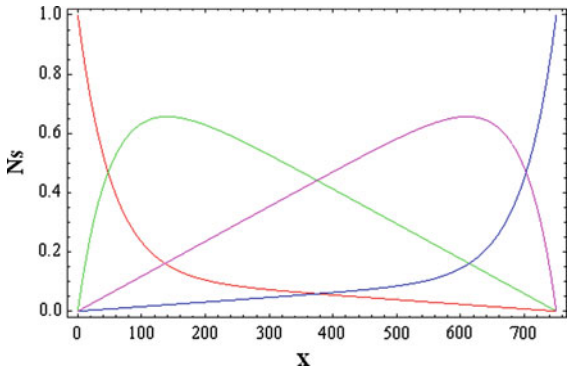

Fig. 18 Steel bar exponential shape functions N_s

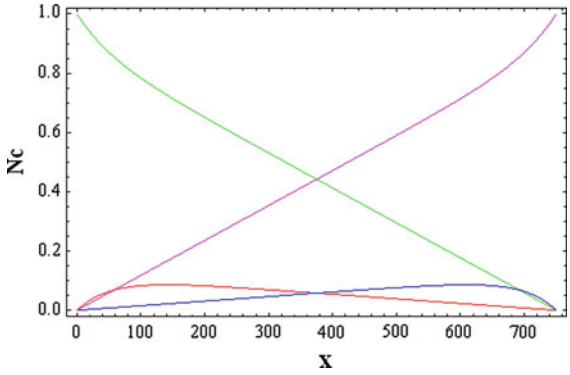

Fig. 19 Concrete exponential shape functions N_c

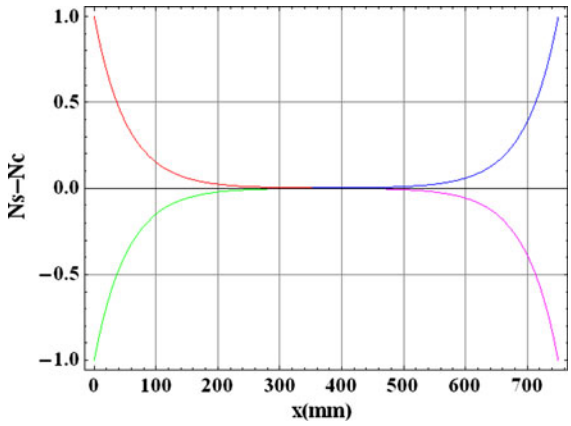

Fig. 20 Slip exponential shape functions $B_g = N_s - N_c$

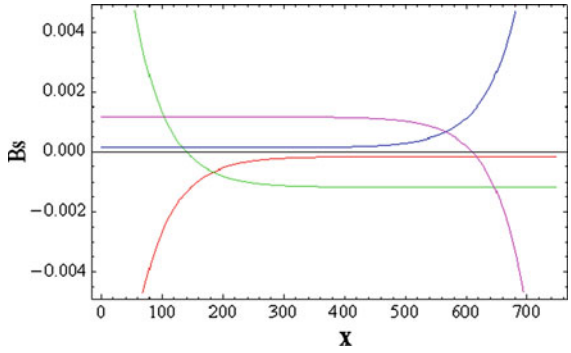

Fig. 21 Derivative of the steel rebar exponential shape functions B_s

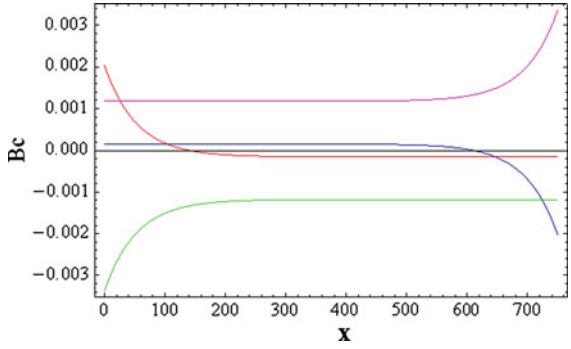

Fig. 22 Derivative of the concrete exponential shape functions B_c

of the discontinuity due to the crack formation. It has been shown that using the standard SDA enhancement it is obtained a stress field with the same degree of continuity as the shape functions across the interface, and this does not always lead to meaningful results.

Therefore an alternative interpolation, based on B-spline bases, has been proposed. These interpolation functions have the same ability as the exponential shape functions for reproducing large stress gradients near the discontinuities. In addition, since splines are not associated to nodal degrees of freedom, but they give a general interpolation, it is very natural to introduce discontinuity in the element, without the need of remeshing and keeping after the crack has opened the same degree of interpolation for the displacement fields. It has been shown how it is possible to introduce a discontinuity using the technique of knot insertion, and similarly it is possible to account for multiple cracks within the same element (this point has not been illustrated in the work). The model presented appears to be accurate in detecting the correct displacement fields, and the computational scheme has proven to be very effective.

The paper has illustrated the general methodology in some detail, so the treatment has been restricted to a beam element. The results suggest that the method can be extended also for developing 2D and 3D elements that account for fibre slipping and crack of the matrix.

Appendix: Exponential shape functions

The exponential shape functions are obtained from the solution (4) of the linearised shear lag problem equation (3), after enforcing the appropriate boundary conditions for each shape functions. The expressions of the shape functions for the steel rebar are:

$$
\begin{aligned}
N_{s_1} &= -\frac{\left(\frac{H}{\alpha^2}+1\right)e^{x\alpha}}{2\left(e^{2L\alpha}-1\right)} + \frac{\left(\frac{H}{\alpha^2}+1\right)e^{2L\alpha-x\alpha}}{2\left(e^{2L\alpha}-1\right)} \\
&\quad + \frac{x\left(H-\alpha^2\right)}{2L\alpha^2} + \frac{\alpha^2-H}{2\alpha^2} \\
N_{s_2} &= \frac{\left(\frac{H}{\alpha^2}+1\right)e^{x\alpha}}{2\left(e^{2L\alpha}-1\right)} - \frac{\left(\frac{H}{\alpha^2}+1\right)e^{2L\alpha-x\alpha}}{2\left(e^{2L\alpha}-1\right)} \\
&\quad + \frac{x\left(-H-\alpha^2\right)}{2L\alpha^2} + \frac{H+\alpha^2}{2\alpha^2} \\
N_{s_3} &= -\frac{\left(\frac{H}{\alpha^2}+1\right)e^{L\alpha-x\alpha}}{2\left(e^{2L\alpha}-1\right)} + \frac{\left(\frac{H}{\alpha^2}+1\right)e^{L\alpha+x\alpha}}{2\left(e^{2L\alpha}-1\right)} + \frac{x\left(\alpha^2-H\right)}{2L\alpha^2} \\
N_{s_4} &= \frac{\left(\frac{H}{\alpha^2}+1\right)e^{L\alpha-x\alpha}}{2\left(e^{2L\alpha}-1\right)} - \frac{\left(\frac{H}{\alpha^2}+1\right)e^{L\alpha+x\alpha}}{2\left(e^{2L\alpha}-1\right)} + \frac{x\left(H+\alpha^2\right)}{2L\alpha^2}
\end{aligned}
$$

The expressions of the shape functions for the concrete core are:

$$
\begin{aligned}
N_{c_1} &= \frac{1}{2}\left(-\frac{\left(\frac{H}{\alpha^2}-1\right)e^{x\alpha}}{e^{2L\alpha}-1} + \frac{\left(\frac{H}{\alpha^2}-1\right)e^{\alpha(L-x)+L\alpha}}{e^{2L\alpha}-1} \right. \\
&\quad \left. + \frac{x\left(H-\alpha^2\right)}{L\alpha^2} - \frac{H}{\alpha^2} + 1 \right) \\
N_{c_2} &= \frac{1}{2}\left(\frac{\left(\frac{H}{\alpha^2}-1\right)e^{x\alpha}}{e^{2L\alpha}-1} - \frac{\left(\frac{H}{\alpha^2}-1\right)e^{\alpha(L-x)+L\alpha}}{e^{2L\alpha}-1} \right. \\
&\quad \left. + \frac{x\left(-H-\alpha^2\right)}{L\alpha^2} + \frac{H}{\alpha^2} + 1 \right) \\
N_{c_3} &= \frac{1}{2}\left(-\frac{\left(\frac{H}{\alpha^2}-1\right)e^{\alpha(L-x)}}{e^{2L\alpha}-1} + \frac{\left(\frac{H}{\alpha^2}-1\right)e^{L\alpha+x\alpha}}{e^{2L\alpha}-1} \right. \\
&\quad \left. + \frac{x\left(\alpha^2-H\right)}{L\alpha^2} \right) \\
N_{c_4} &= \frac{1}{2}\left(\frac{\left(\frac{H}{\alpha^2}-1\right)e^{\alpha(L-x)}}{e^{2L\alpha}-1} - \frac{\left(\frac{H}{\alpha^2}-1\right)e^{L\alpha+x\alpha}}{e^{2L\alpha}-1} \right. \\
&\quad \left. + \frac{x\left(H+\alpha^2\right)}{L\alpha^2} \right)
\end{aligned}
\tag{33}
$$

In Eqs. (33), (33) symbols L, α, H denote

$$
\alpha = \sqrt{G_0 \pi \phi_s \left(\frac{1}{E_s A_s} + \frac{1}{E_c A_c} \right)} \tag{34}
$$

$$
H = G_0 \pi \phi_s \left(\frac{1}{E_s A_s} - \frac{1}{E_c A_c} \right) \tag{35}
$$

Figures 18, 19 show a plot of these functions for some choice of the mechanical and geometrical parameters. Note that, due to the presence of the slip, steel as well concrete displacements depend on all of the the nodal degrees of freedom.

Particularly, from the plots of the deformation shape functions B_s, B_c in Figs. 20, 21, 22 it is apparent that the exponential shape functions have the property of concentrating the deformations at the ends of the element.

References

Alfaiate J, Simone A, Sluys L (2003) Non-homogeneous displacement jumps in strong embedded discontinuities. Int J Solids Struct 40:5799–5817

Auricchio F, Beirão da Veiga L, Buffa A, Lovadina C, Reali A, Sangalli G (2007) Isogeometric finite element data structures based on bzier extraction of nurbs. Comput Methods Appl Mech Eng 197:160–172

Ayala G, Contrafatto L, Cuomo M, Retama J (2010) Consistent symmetric formulation of the enhanced embedded discontinuity method. In: IV European conference on computational mechanics

Barenblatt GI (1962) The mathematical theory of equilibrium cracks in brittle fracture. Adv Appl Mech 7:55–129

Becker G, Noels L (2011) A fracture framework for euler-bernouilli beams based on a full discontinuous Galerkin formulation/extrinsic cohesive law combination. Int J Numer Methods Eng 85:1227–1251

Belytschko T, Moës N, Usui S, Parimi C (2001) Arbitrary discontinuities in finite elements. Int J Numer Methods Eng 50:993–1013

Benson D, Bazilevs Y, Hsu MC, Hughes TJR (2011) A large deformation, rotation free, isogeometric shell. Comput Methods Appl Mech Eng 200:1367–1378

Borden MJ, Scott MA, Evans KA, Hughes TJR (2011) Isogeometric finite element data structures based on bzier extraction of nurbs. Int J Numer Methods Eng 87:15–47

Caballero A, Carol I, López CM (2007) 3D meso-mechanical analysis of concrete specimens under biaxial loading. Fatigue Fract Eng Mater Struct 30(9):877–886

CEB-FIP: Model Code 90. Thomas Telford Ltd, 1993

Chudoba R, Jerabek J, Peiffer F (2009) Crack-centered enrichment for debonding in two-phase composite applied to textile reinforced concrete. Int J Multiscale Comput Eng 7(4):309–328

Choi CK, Kim KH, Hong HS (2002) Spline finite strip analysis of prestressed concrete box-girder bridges. Eng Struct 24:1575–1586

Ciancio D, Carol I, Cuomo M (2007) Crack opening conditions at corner nodes in FE analysis with cracking along mesh lines. Eng Fract Mech 74:1963–1982

De Luycker E, Benson D, Belytschko T, Bazilevs Y, Hsu M (2011) X-FEM in isogeometric analysis for linear fracture mechanics. Int J Numer Methods Eng 87:541–565

Dias-da Costa D, Alfaiate J, Sluys L, Júlio E (2009) Towards a generalization of a discrete strong discontinuity approach. Comput Methods Appl Mech Eng 198:3670–3681

Dias-da Costa D, Alfaiate J, Sluys L, Júlio E (2010) A comparative study on the modeling of discontinuous fracture by means of enriched nodal and element techniques and interface elements. Int J Fract 161:97–119

Dugdale DS (1960) Yielding of steel sheets containing slits. J Mech Phys Solids 8(2):100–104

Eve R, Reddy B, Rockafellar R (1990) An internal variable theory of elastoplasticity based on the maximum plastic work inequality. Quart Appl Math 48:59–83

Huang H, Costanzo F (2004) On the use of space-time finite elements in the solution of elasto-dynamic fracture problems. Int J Fract 127(2):119–146

Ibrahimbegovic A, Boulkertous A, Davenne L, Brancherie D (2010) Modelling of reinforced-concrete structures providing crack-spacing based on X-FEM, ED-FEM and novel operator split solution procedure. Int J Numer Methods Eng 83:452–481

Jirásek M, Zimmermann T (2001) Embedded crack model: part i: basic formulation. Int J Numer Methods Eng 50:1269–1290

Keuser M, Mehlhorn G (1987) Finite element models for bond problems. J Struct Eng 113:2160–2173

Kiendl J, Bletzinger K, Linhard J, Wuchner R (2009) Isogeometric shell analysis with Kirchhoff-Love elements. Comput Methods Appl Mech Eng 198:3902–3914

Lachner R, Mang H (2003) Scale transition in steel–concrete interaction. I: model. J Eng Mech ASCE 129(4):393–402

Liao K, Reifsnider L (2000) A tensile strength model for unidirectional fiber-reinforced brittle matrix composite. Int J Fract 106:95–115

Linder C, Armero F (2007) Finite elements with embedded strong discontinuities for the modeling of failure in solids. Int J Numer Methods Eng 72:1391–1433

Moës N, Dolbow I, Belytschko T (1999) A finite element method for crack growth without remeshing. Int J Numer Methods Eng 46:131–150

Mosler J (2005) A novel algorithmic framework for the numerical implementation of locally embedded strong discontinuities. Comput Methods Appl Mech Eng 194:4731–4757

Newmark NM, Siess CP, Viest IM (1951) Tests and analysis of composite beams with incomplete interaction. In: Proceedings of society for experimental stress analysis, vol 9, pp 75–92

Oliver J (1996) Modelling of strong discontinuities in solid mechanics via strain softening constitutive equations. Part 1: fundamentals. Part 2: numerical simulation. Int J Numer Methods Eng 39(21):3575–3623

Ortiz M, Leroy Y, Needleman A (1987) A finite element method for localized failure analysis. Comput Methods Appl Mech Eng 61:189–214

Oliver J, Cervera M, Manzoli O (1999) Strong discontinuities and continuum plasticity models: the strong discontinuity approach. Int J Plast 15:319–351

Oliver J, Huespe A, Snchez P (2006) A comparative study on finite elements for capturing strong discontinuities: E-FEM vs. X-FEM. Comput Methods Appl Mech Eng 195:4732–4752

Oliver J, Linero D, Huespe A, Manzoli O (2008) Two-dimensional modeling of material failure in reinforced concrete by means of a continuum strong discontinuity approach. Comput Methods Appl Mech Eng 197:332–348

Prasad M, Krishnamoorthy C (2002) Computational model for discrete crack growth in plain and reinforced concrete. Comput Methods Appl Mech Eng 191:2699–2725

Prechtel M, Leiva Ronda P, Janish R, Hartmaier A, Leugering G, Steinmann P, Stingl M (2011) Simulation of fracture in heterogeneous elastic materials with cohesive zone models. Int J Fract 168:15–29

Radtke F, Simone A, Sluys L (2011) A partition of unity finite element method for simulating non-linear debonding and matrix failure in thin fibre composites. Int J Numer Methods Eng 86:453–476

Rockafellar R (1970) Convex analysis. Princeton University Press, Princeton, NJ

Simo JC, Oliver J (1994) A new approach to the analysis and simulation of strain softening in solids. In: Bažant ZP, Bittnar Z, Jirásek M, Mazars J (eds) Fracture and damage in quasi-brittle structures. E&FN Spon, London, pp 25–39

Simo J, Oliver J, Armero F (1993) An analysis of strong discontinuities induced by strain softening in rate independent inelastic solids. Comput Mech 12:277–296

Verhoosel C, Scott M, de Borst R, Hughes TJR (2011) An isogeometric approach to cohesive zone modeling. Int J Numer Methods Eng 87:336–360